PVDF/h-BN hybrid membranes and their application in desalination through AGMD

Rasoul Moradi*[1,2], Mojtaba Shariaty-Niassar[2a], Nazila Pourkhalili[1b], Masoud Mehrizadeh[1c] and Hassan Niknafs[1d]

[1]*Department of Chemical Engineering, School of Engineering and Applied Science, Khazar University, Azerbaijan*
[2]*Transport Phenomena & Nanotechnology Laboratory, School of Chemical Engineering, College of Engineering, University of Tehran, Iran*

Abstract. A new procedure to produce poly(vinylidene fluoride)/boron nitride hybrid membrane is presented for application in membrane distillation (MD) process. The influence of hexagonal boron nitride (h-BN) incorporation on the performance of the polymeric membranes is studied through the present investigation. For this aim, h-BN nanopowders were successfully synthesized using the simple chemical vapor deposition (CVD) route and subsequent solvent treatments. The resulting h-BN nanosheets were blended with poly(vinylidene fluoride) (PVDF) solution. Then, the prepared composite solution was subjected to phase inversion process to obtain PVDF/h-BN hybrid membranes. Various examinations such as scanning electron microscopy (SEM), wettability, permeation flux, mechanical strength and liquid entry pressure (LEP) measurements are performed to evaluate the prepared membrane. Moreover, Air gap membrane distillation (AGMD) experiments were carried out to investigate the salt rejection performance and the durability of membranes. The results show that our hybrid PVDF/h-BN membrane presents higher water permeation flux (~18 kg/m^2 h) compared to pristine PVDF membrane. In addition, the experimental data confirms that the prepared nanocomposite membrane is hydrophobic (water contact angle: ~103˚), has a porous skin layer (>85%), as well competitive fouling resistance and operational durability. Furthermore, the total salt rejection efficiency was obtained for PVDF/h-BN membrane. The results prove that the novel PVDF/h-BN membrane can be easily synthesized and applied in MD process for salt rejection purposes.

Keywords: membrane distillation; polymers; salt rejection; water treatment; flux

1. Introduction

1.1 MD technology for desalination

Seawater desalination is a potential way out to the perilous state of the future water needs backup (Moradi *et al.* 2016a, b). Hence, a great number of research is ongoing for the development of novel separation technologies, especially in the field of membrane based desalination processes (Al-Shammiri *et al.* 2000, Bottino *et al.* 2015, Huayan *et al.* 2011).

Membrane Distillation (MD) method has cached great interest due to its potential advantages on energy consumption, simplicity and its potential to be coupled with solar energy (Van der Bruggen *et al.* 2003, Koo *et al.* 2013, Chang *et al.* 2015). MD technology can be adapted effectively for water desalination and treatment in industrial applications. In this process, a difference in partial vapor pressure of feed components serves as the driving force and the presence of a hydrophobic membrane ensures vapor permeation and condensation in the product side (Al-Obaidani *et al.* 2008). A hydrophobic membrane as an interface between feed and permeate streams allowing the vapor phase molecules to pass through the membrane's pores. Various types of MD techniques have been developed manly based on the arrangement and operation manner of the permeate side of the MD module. The main four MD techniques are Direct Contact MD (DCMD), Air Gap MD (AGMD), Sweeping Gas MD (SGMD) and Vacuum MD (VMD) (Moradi *et al.* 2016). Comparatively DCMD is the most developed MD method due to its simplicity and high permeate flux. In DCMD both sides of MD membrane directly are in contact with liquid hot-feed and liquid-coolant streams (Criscuoli *et al.* 2013, Loussif *et al.* 2016). Furthermore, in many DCMD applications feed hot-side temperatures under 90°C are suitable; hence, this process is ideal for exploiting waste heat or solar thermal resources (Criscuoli *et al.* 1999, Darwish *et al.* 2000). However, many obstacles remain before this technology becomes applicable in industry (Guillén-Burrieza *et al.* 2011).

1.2 Membranes of MD process

The main challenges in MD process are relevant to the employed membrane natural drawbacks such as low durability and permeation flux. For this reason, fabrication of the modified membrane to obtain higher efficiency plays an important role in commercializing of this method (Lau *et al.* 2011). Various procedures such as nano-compositing and surface engineering have been reported in literature to

---

∗Corresponding author, Professor
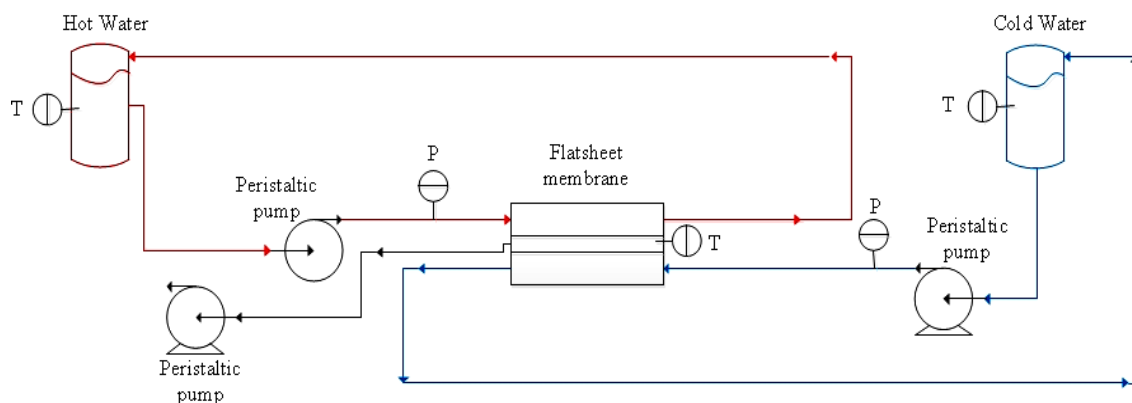 E-mail: rmoradi@khazar.org

Fig. 1 AGMD flow diagram used for permeation flux and desalination tests

synthesize efficient MD membranes (Khayet *et al*. 2005). Poly(vinylidene fluoride) (PVDF) is one of the main materials that extensively applied in preparation of MD's specific membranes. Meanwhile PVDF-inorganic hybrid membranes e.g., PVDF/TiO$_2$, PVDF/SiO$_2$, PVDF-nanocarbon composite membranes e.g., PVDF/carbon nanotube, PVDF/graphene, possess modified properties in comparison to pristine membranes. Therefore, implementation of novel and cost-effective nanomaterials for preparation of efficient MD membranes is flourishing field of investigation (Qtaishat *et al*. 2009).

Surface modification of the MD membranes is an efficient method for inducing the desired properties. As an interface between the bulk of the membrane and the environment, surface of membrane is the very active research area due to its straight influence on the many applicable properties. Especially the surface of the polymeric materials plays the key role to determine the very specific features such as wettability, roughness, adhesion, durability, biocompatibility, etc. (Moradi *et al*. 2015, Moradi *et al*. 2017). For instance, in the field of membrane science, the surface properties of the polymeric membranes recognize the class of application namely nanofiltration, microfiltration, reverse osmosis, membrane distillation etc. However, the pristine surface of the membranes sometimes doses not satisfy the desired performance. Therefore, the required properties of the surface often demand special molecular structures, which could not be fulfilled by the employed polymer chemical structure. The surface modification presents the effective way to obtain the acceptable surface of the membrane to extend its application. This is an important issue in the new emerging process of membrane distillation, for which there are not appropriate commercial membranes and MD generally employs the microfiltration membranes. Hence, the MD specific membranes usually are prepared in the research laboratories for specific investigations such as surface modifications (Zoungrana *et al*. 2016).

In many cases addition of modifiers such as nanomaterials and surface modifying macromolecules (SMMs), transforms the membrane into a composite bilayered form with dual characteristics. Because SMMs migrate to the top surface, induce higher hydrophobicity, i.e., high water contact angle, to this surface compared to the bulk of membrane and its bottom surface. In fact, the terminal fluorine groups orient towards the surface of the blend, resulting in diminishing of the surface energies. In addition, the morphological difference (skin top-layer and porous sub-layer) is created across the membrane because of SMMs concentration gradient across the membrane width (Shoaii *et al*. 2017).

Recently hexagonal boron nitride (h-BN) has captured attention of many researchers with interests in polymeric composites. h-BN nano-powder has a great potential to be used as an additive to strengthen the polymer matrix and induce novel characteristics. This is due to h-BN exclusive properties such as high thermal conductivity, mechanical robustness, exceptional resistance to oxidation mainly because it is iso-structural with graphene (Fig. 1) (Shi *et al*. 2004, Duan *et al*. 2008, Hossain *et al*. 2013). Mixing of h-BN nanopowders with some materials such as ceramics, alloys, resins, plastics and rubbers can induce them with desirable properties. In fact, h-BN nanosheets are the analogue of the graphene then it is known as the white graphene and could indicate the similar characteristics (Hao *et al*. 2002, Zhi *et al*. 2005, Ciofani *et al*. 2008).

Preparation of polymer/h-BN composites are the topic of various studies in the literature (Zhi *et al*. 2006, Choi *et al*. 2007, Moradi *et al*. 2017). However, there are not remarkable works in the field of preparation and characterization of polymer/h-BN hybrid membranes. Intrinsic properties of h-BN nanosheets such as high hydrophobicity and mechanical strength can improve the polymeric membrane efficiencies. Specially in MD process, wherein membranes suffer from law permeation fluxes. Moreover, increasing in the membrane porosity for obtaining higher permeation fluxes brings out various drawbacks such as fragility of the membrane (Khayet *et al*. 2005). Hence, increasing in the MD permeation flux with fewer side effects is worthy to be investigated. Preparation and employing composite membranes like PVDF/h-BN in MD process is an appropriate route to tackle these problems (Smolders *et al*. 1989, Hubacek *et al*. 1996, Hubacek *et al*. 1994)

Here, through the compositing of PVDF with h-BN we present a new hybrid membrane with potential application in membrane distillation process. Firstly, mono-layered h-BN nanosheets are prepared using CVD reactor, then synthesized powder with further purification was added in appropriate weigh ratio to the PVDF casting solution. Secondly the phase inversion method is used to prepare the

hybrid membrane in various desired thicknesses. Finally, the prepared PVDF/h-BN membrane is examined on the permeation, durability and hydrophobisity properties. It should be mentioned that the air gap membrane distillation process was employed to achieve this goal. The results indicate that the PVDF/h-BN membrane compared to pristine PVDF membrane, exhibits some superior properties at membrane distillation operational conditions.

2. Materials and method

2.1 h-BN synthesis

BN precursor samples were prepared using 6.962 g of boric anhydride (B_2O_3, 99.95%, Sigma-Aldrich Co., U.S.A) dissolved in 500 ml of methanol at 25°C. After dissolution, 9.553 g of Guanidine hydrochloride (CH_5N_3.HCl, 99.98%, Sigma-Aldrich Co., U.S.A) was slowly added to the medium under agitation. The prepared samples were allowed to stand for 24 hours at room temperature. Then it was filtered and dried at 35°C. The product obtained is $B_4N_3O_2H$, which is the precursor to BN. This precursor material was heated in vacuum oven without gas flow at 250°C for 5 hours constantly. The obtained white salt was placed in a quartz boat and loaded into the tubular CVD reactor then heated at 1100°C (10°C/min) for 2 hours under nitrogen-hydrogen (9:1) gas flow. The prepared h-BN powder is subjected to a series of solvent assisted ultrasonic treatments to perform single layer transformation.

For this purpose, 2.00 g of the unrefined h-BN powder is mixed in 10ml methanol solution and sonicated for about 1 hour. The achieved suspension is centrifuged and decanted to eliminate dissolved salts such as the remaining B_2O_3. This procedure was repeated and the product was leached using diluted HCl (1.0 wt.%) in order to remove the trace metallic contaminations. Finally, the purified h-BN is dried at 200°C overnight and is prepared for exfoliation experimenters. The obtained multilayer h-BN is characterized and then subjected to ultrasound treatment in isopropanol (IP). 1.00 g of h-BN is added to 5.0 ml IP and sonicated for 24 hours. The increasing of interlayer distance is investigated using micro-Raman spectroscopy.

2.2 Membrane preparation and operation

Poly(vinylidene fluoride) (PVDF with 400,000-600,000 molecular weights, Sigma Aldrich, U.S.A) was dissolved in dimethylformamide (DMF, Sigma Aldrich, U.S.A) to prepare 13 wt.% of polymer solution. The synthesized single layer bulky h-BN was mixed in appropriate weight ratio (0.001 wt.%) to the polymer solution. The prepared precursor solution was casted in methanol/water (20:80 v/v) bath at 25°C. After rinsing it by methanol it was dried in 50°C. The prepared hybrid PVDF/h-BN membranes are characterized and employed in the following air gap membrane distillation (AGMD) examinations.

The prepared h-BN and membrane samples were characterized by Fourier-transform infrared spectroscopy (FTIR) (Brucker 3020, Germany) ranging from 4000 to 400 cm^{-1} at room temperature, X-ray diffraction (XRD, Instron,

Table 1 Operational parameters for AGMD unite cell experimentation using synthetic PVDF and PVDF/h-BN membranes

Parameter	Value
Coolant temperature (°C)	20
Coolant flow rate (ml/min)	300
Feed flow rate (ml/min)	200
Air gap thickness (mm)	5
Air gap pressure (kPa)	100
Membrane effective area (cm^2)	30

France) with a Cu-Ka tube and scanning electron microscopy (SEM, JEOL, Hittachi, Japan) operating at 30 kV. The roughness values of the membranes were measured using atomic force microscopy (AFM) (FemtoScan, Russia). The mechanical characteristics of membranes were studied using a universal testing machine (AGS-J 500 N, Shimadzu, Tokyo, Japan) at room temperature according to ASTM D638-10. Thermal properties were evaluated by employing ddifferential scanning calorimeter (DSC, TA Instruments, DE, U.S.A).

A flat-sheet AGMD module of 30 cm length and 20 cm width was manufactured and employed in experiments. To maintain high thermal and mechanical stability for long-term operations High-density PTFE materials is used in the module fabrication. The effective membrane area in this module was 30 cm2. The schematic representation of the AGMD setup is shown in Fig. 1. In the AGMD configuration, the peristaltic pumps were employed to take out the permeate stream which caused a relative vacuum in the module air gap section (~100 kPa). Vacuum is measured using vacuum gage (Aut-Meter 4303) that is interposed on the module-permeate stream outlet. Hence, we labelled this AGMD setup a vacuum enhanced AGMD. The feed and coolant stream temperature were stabilized at 75°C and 20°C, respectively.

The MD experiments established the best compromise among different parameters such as permeate flux, separation efficiency, etc. Optimized values of temperatures, flow rates and pressures were applied in all AGMD experimentations. Operational parameters were listed in Table 1. For precise measuring of the permeate flux the weighing method is employed. A high accuracy analytical balance was used to determine permeation flux from module air gap.

2.3 Membrane mechanical test

The dynamic mechanical analysis (DMA) of membranes was performed using universal tensile test machine (Sanwood technology Co., Guang Dong, China) at ambient temperature. Prepared films were subjected to strain-stress measurements using tensile tester. Young's modulus and elongation at breaking point were studied for both hybrid PVDF/h-BN and pristine PVDF membranes. The embranes were cut into 10 mm (width) × 50 mm (length) test strips for DMA analyses.

3. Results and discussion
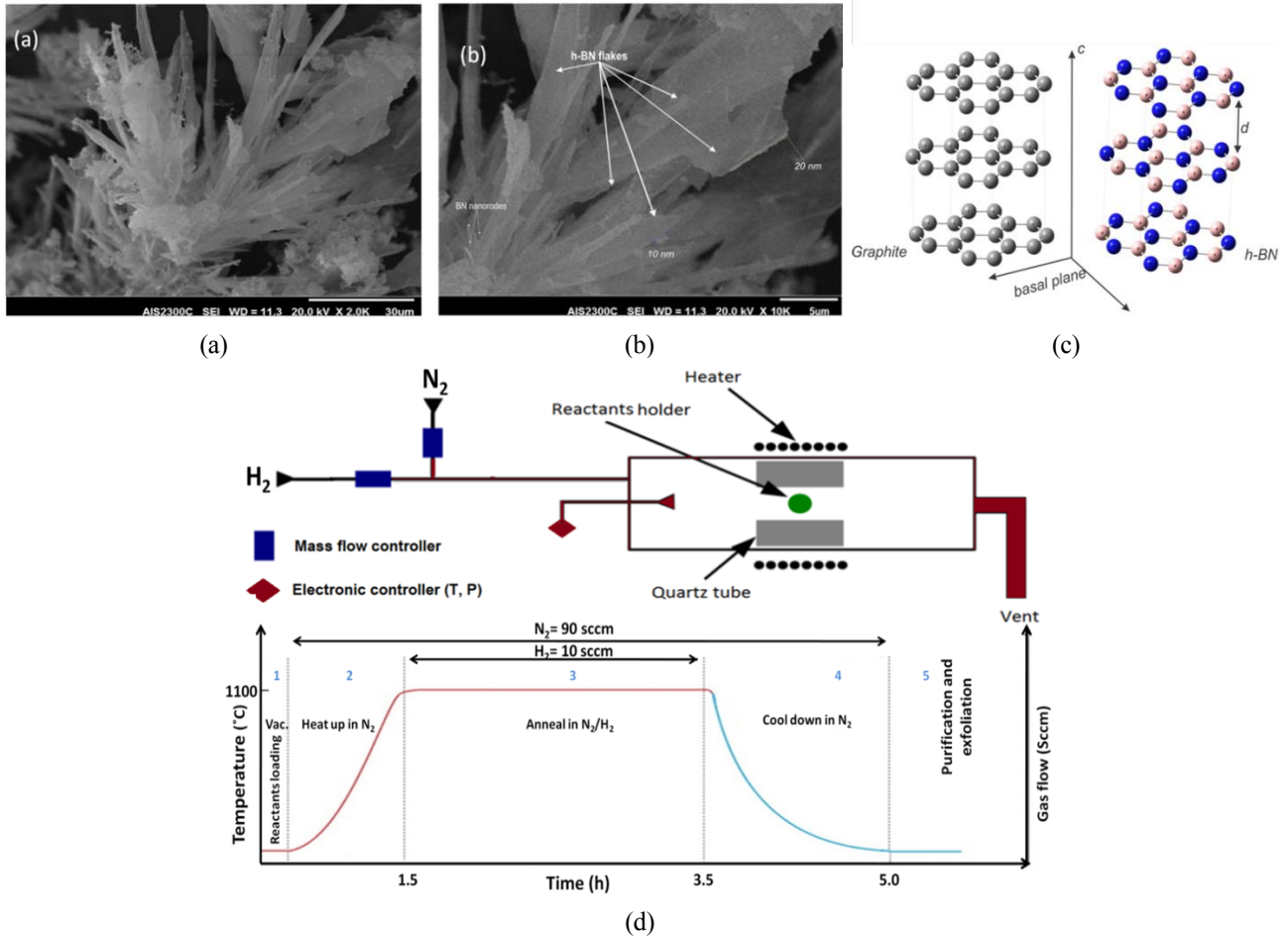
(a)   (b)   (c)

(d)

Fig. 2 (a) XRD spectra of CVD precursor and h-BN product, (b) FTIR spectroscopy pattern for produced BN powder and the precursor subjected to CVD, (c) SEM image of purified h-BN nanopowder, (d) Raman spectra of produced h-BN

3.1 h-BN synthesis and characterization

Fig. 2 outlines the simple CVD reactor and relevant conditions for four operation steps that are used throughout the process and the SEM micrographs of synthesized h-BN. The h-BN is synthesized at 1100˚C in customized cold-wall CVD reactor. As shown, the product of boric acid and guanidine hydrochloride reaction, is loaded into the CVD quartz tube in an appropriate quartz holder. Following the process diagram in Fig. 2(d), the BN powder is produced as the precipitation in the cold ends of the quartz tube. Initially, the sample is vacuumed in CVD and its temperature is gradually increased to 1100˚C within 1.5 hours. As depicted in in Fig. 2 the third step is named annealing and synthesizing of BN powder is commenced in the respect step. Then, the fourth step is allocated to cooling BN powder and finally purification and exfoliation of BN powder is occurred at the fifth step. The steps of 1 to 4 and with 3 are done under N2 and H2 stream with the flow rates of 90 sccm and 10 sccm, respectively. As produced BN powder is collected and characterized. In addition, the prepared powder is purified for exfoliation experiments.

SEM images of h-BN synthesized in the CVD are shown in the in Fig. 2(a). These micrographs reveal that the bulk of as-prepared h-BN powder include the flakes with irregular shapes and different range of thicknesses. In addition, Fig. 2(b) presents adequate exfoliation for h-BN powders. It declares that these flakes are like the booming flowers. Other phases of BN such as amorphous BN and h-BN platelets along with nanorods are observed in Figs. 2(a) and 2(b). However, the amounts of these kinds of BN are in minority in comparison to h-BN phase and can be eliminated through some leaching experiments. Therefore, h-BN powders which were synthesized by CVD can be applied for further process, exfoliation, to obtain mono layer h-BN.

The XRD pattern of as-produced h-BN and relevant precursor is shown in in Fig. 3(a). Besides, h-BN specific diffraction peaks, it shows various peaks corresponding to different phases of boron nitrides such as c-BN and the salty contaminants like B_2O_3. The two h-BN specific peaks at around 2θ=26˚ and 41˚ indicate that the CVD product contains favoured h-BN platelets (Smolders *et al*. 1989).

From the diffraction spectrum, the approximate size of the synthesized h-BN particles could be calculated using the Scherrer equation (Hubacek *et al*. 1996), which is given by

$$D_{hkl} = K\lambda / b_{hkl} \cos q_{hkl} \qquad (1)$$

Wherein *hkl* are called Miller indices for correspondent crystalline plane of identified diffraction peak, D_{hkl} is the particle size perpendicular to unit cell normal line of (*hkl*)

plane, *K* is dimensionless shape factor (of around 0.9), b_{hkl} is width at half height of (*hkl*) diffraction peak and *λ* is wavelength of X-ray (typically 1.54 A˚).

Figs. 3(b) and 3(d) show the FTIR and micro Raman spectra of the CVD reactants used as h-BN precursor and the produced h-BN powder. The synthesized h-BN absorption features could be interpreted considering the sp^2-bonds in comparison with other forms of BN such as c-BN. As shown the vibration fingerprint of the CVD obtained product is different from the loaded precursor peaks appearance near 780 and 1370 cm^{-1} are the fingerprint of sp^2-bonded h-BN. The 1370 cm^{-1} mode is a stretching of the BN bond within the basal plane and the 780 cm^{-1} mode is a bending of the B-N-B bond in between the basal planes.

The observed shoulder-like bands at around 1100 and 1170 cm-1 are attributed to the sp3-bonded BN which appear due to the formation of amorphous boron nitride and other crystalline phases (c-BN, r-BN and w-BN) as shown in SEM micrographs of in Figs. 3(a) and 3(b). As illustrated in SEM micrographs, various BN forms exist in the synthesized powder. However, the main portion of the synthesized powder contains h-BN flakes with wide ranges of dimension and thickness. The thicknesses of the h-BN flakes measured to be at around 10-20 nm and the determined mean size of them is around 5-50 μm2. One important feature of the obtained SEM images is the existence of rod-like structures of BN from nano-size to a few micrometers. BN nanorods are characteristic of r-BN crystalline forms that rarely produce at 1100˚C during the CVD synthesize process. The none-reacted precursor salts such as B2O3 etc. ale also observed in SEM images. These observations indicate that the synthesized h-BN powder include impurities and must undergo further purification before subjecting to sonication and exfoliation.

3.2 PVDF/h-BN membrane characterization

SEM micrographs of synthesized membranes are represented in Figs. 4 and 5. As is shown with addition of h-BN in the precursor polymer solution, the average pore size of synthesized membrane increased, the morphology of the membrane changed and consequently other membrane properties differed significantly.

The surface morphology of the pristine PVDF membrane is represented in Fig. 4. The formation of dense skin layer in this case is the main reason for the low achievable operational fluxes. In comparison with the SEM images of the PVDF/h-BN hybrid membrane (from Figs. 5(a) and 5(b)), the skin layer is removed due to the compositing effects of h-BN platelets. This is due to accumulation of the polymer chains on the h-BN nanosheets, which induce the grain-like morphology to prohibit the dense layer formation on the surface of PVDF/h-BN membrane. Interposing of the PVDF chains among the h-BN platelets construct a physical network that basically induces molecule relaxation and microscopically repackages the polymeric chains. This effect tends to improve chains packing in coagulation process and enhance the porosity of the selective skins and minimize the surface defects (Chung *et al*.1996, Moradi *et al*. 2015).

The compositing effect in the case of interposing 2D platelets e.g. Graphene and h-BN nanosheets, could be

Table 2 Comparative properties of the PVDF and PVDF/h-BN membranes

Membrane	Mean pore size (μm)	Max pore size (μm)	Contact angle (°)	Roughness R_a (nm)	Porosity (%)	LEP kPa
PVDF	0.19±0.048	0.30±0.051	87±2.0	70	63±5.4	220±9.6
PVDF/h-BN	0.22±0.052	0.50±0.046	103±1.9	240	81±4.8	250±10.1

described by crystallographic studies (Wu *et al*. 2016, Dastbaz *et al*. 2017, Moradi *et al*. 2015). The incorporation of h-BN platelets induced the PVDF crystal transformation from γ-form to α-form and resulted in a more open and loose sublayer structure (Zha *et al*. 2011, Yu *et al*. 2015). It results in integrating of skin layer to sublayer and formation of symmetric structure with uniform pores wherein skin layer is totally removed or becomes ultra-thin. In addition, the agglomeration of polymer chains on in adjacent zones of h-BN platelets enhance the formation of uniform pores across the overall membrane. Furthermore, the addition of h-BN in the PVDF can lead to surface morphological changes by influencing the crystallization of PVDF to form porous PVDF materials with rough surfaces, resulting in increasing hydrophobicity.

The closer representations of PVDF/h-BN membrane at Fig. 5(c) and 5(d) illustrate that the pore sizes of the membrane are increased and the polymeric beads shape the major surface structure of the membrane.

Liquid entry pressure (LEP) results show that for the hybrid membrane greater hydrostatic pressure could be applied; this is mainly due to its increased hydrophobic characteristics rather than pore size. On the other hand, considering large pore size of PVDF/h-BN membrane the measured LEP values expected to be low compared to pristine PVDF membrane. However, significant increasing in its hydrophobicity compensates the pore size increasing effect and results in higher LEP values.

The following equation is used to calculate permeation flux of the membranes.

$$J = \frac{W}{A.t} \tag{2}$$

Where J is the pure water flux (Kg/(m^2·h)), W is the permeation mass of water (Kg), A is the effective membrane areas (m^2), t is the sampling time (h). The solute rejection (R) of membrane was obtained from the following equation.

$$R = \left(1 - \frac{c_1}{c_2}\right) \times 100\% \tag{3}$$

Where C_1 and C_2 are the solute concentration of permeate and feed solution, respectively that measured by water quality meter (Model 900, BANTE Co., China).

Table 2 shows the main properties of the PVDF/h-BN membrane in comparison with pristine PVDF membrane. As expected from SEM images, the measured mean pore size and maximum pores sizes of the PVDF/h-BN membrane measured to be around 0.22 and 0.5 μm, respectively; which are greater than PVDF pore size values. Water contact angle results demonstrate that the h-BN addition into PVDF membrane intensify the hydrophobicity properties. Wherein the water contact angle of the PVDF

membrane is about 87°, for the PVDF/h-BN membrane this value is obtained to be 103° (Fig. 4(b)). The membranes roughness was obtained from surface profilometry measurements and average values are represented in Table 2.

The porosity measurement results prove the observation of SEM images in which the porosity of the PVDF/h-BN membrane, was about 81% and for the pristine PVDF it was around 63%. As mentioned earlier, the differences between the membranes porosities are directly related to the presence of h-BN platelets in the polymer matrix. h-BN platelets remove the skin layer and induce the beaded morphology with spongy structure. The introduced microstructure of the PVDF/h-BN membranes creates the higher roughness on the surface. However, this kind of structure may suffer from the mechanical strength drawbacks. Hence, the durability of the membranes is examined and the results are as follow:
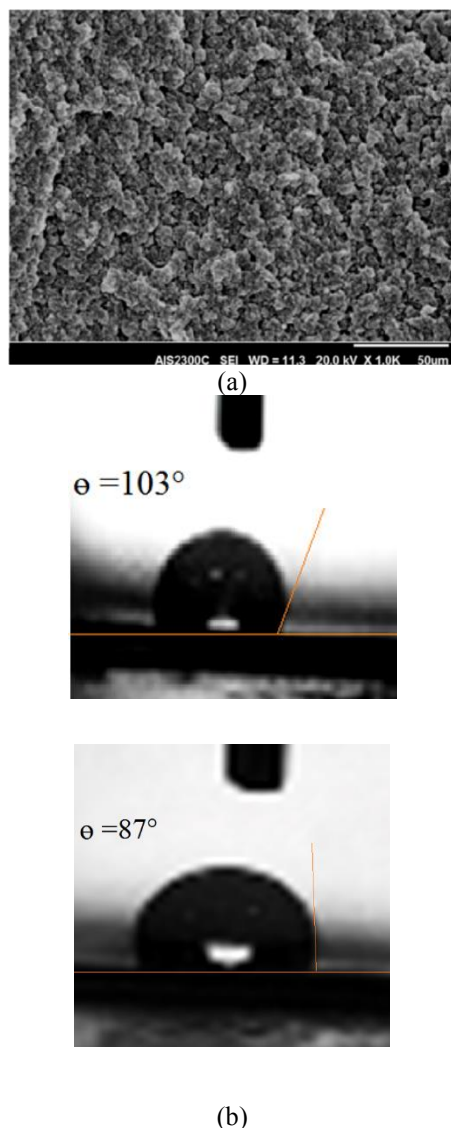

(a)

(b)

Fig. 4 (a) SEM representation of PVDF membrane skin layer prepared through casting in methanol bath at 25°C. (b) Water contact angle images of PVDF/h-BN membranes (left, CA=103°) and pristine PVDF membrane (right, CA=87°)

The formation mechanism of PVDF/h-BN porous-nanocomposite membrane in the casting process of the present work, is similar to that described by Zha *et al*. (Zha *et al*. 2011, Yu *et al*. 2015). Wherein the pristine PVDF membrane forms through a liquid-liquid de-mixing process while the composite PVDF/h-BN. Indeed, membrane forms by a solid-liquid segregation, where h-BN nanosheets are acting as crystallization nuclei which are boosting the solid-liquid de-mixing process. As a conclusion the incorporation of h-BN nanosheets into PVDF polymer matrix does not only change the pore size and surface morphology but also influences the crystallization, i.e., enhancing α-form PVDF crystals (Yu *et al*. 2015).

3.3 AGMD experiments

3.3.1 Feed temperature effect on AGMD flux

The effect of feed temperature on permeation flux of the membranes was studied in series of AGMD experiments to evaluate the membranes performance in different feed temperatures. These experiments were carried out with feed concentration of 1.00 molar NaCl and feed flow rate of 200 ml/min. The obtained results for permeation fluxes are illustrated in Fig. 6(a) for both types of membranes. As shown, the permeation fluxes of membranes are increased when temperature is raised in the feed stream. However, the fluxes of synthesized PVDF/h-BN membrane experiences more increasing with temperature in comparison with pristine membrane. With applied coolant temperature of 20°C and feed temperature of 25°C, the same value of 5.20 kg/m2h was obtained for membranes. When the feed temperature was increased to 55°C, the permeation flux of PVDF/h-BN membrane reached to 11.65 kg/m2h compared to 9.50 kg/m2h for PVDF membrane. Also at the maximum feed temperature of 70°C, the difference in permeation fluxes was observed to be 12.75 kg/m2h for pristine and 18.10 kg/m2h for hybrid membrane. The rise in the feed temperature enhance the vapor formation and diffusion in the membrane pores and as a result it increases the permeate flux of both membranes. However, the obtained trends for permeation flux variation with feed temperature indicate that the PVDF/h-BN membrane is more sensitive to temperature when compared to PVDF membrane. The main explanation for this observation is that the addition of h-BN flakes increases the thermal expansion property of the membranes (Lee *et al*. 2006, Kim *et al*. 2008). Considering the wide range of pore sizes in PVDF/h-BN membrane, increase in temperature induces an expansion to the size of meso-sized pores (greater than 50nm), as well as, the contraction in the spacious of a few micrometer-sized pores. This temperature increasing effect, causes an appropriate variation in the pore sizes of PVDF/h-BN resulting more rising in the permeate fluxes compared to PVDF membrane. Furthermore, the ceramic nature of h-BN strengthens the pores mechanical strength, which results in less ruptures in the pore structures of PVDF/h-BN membrane at high temperatures. On the other hand, for pristine PVDF, the fragile structure of membrane pores results in their destruction and closure at high temperatures.

3.3.2 Feed flow rate on AGMD flux

To evaluate the membranes performance in different feed flow rates, influence of this parameter variation on permeation flux of the membranes were investigated in AGMD experiments. These experiments were carried out with feed concentration of 20 g/l NaCl and feed temperature of 70˚C. The obtained results for permeation fluxes are illustrated in Fig. 6(b) for both types of membranes. As shown, the permeation flux is increased when the flow rate of feed stream is increased. This is due to increase in the hydrostatic pressure across the membrane, which amplify the diffusion mechanisms of feed molecules into the membrane pores. However, the observed salt rejection results for both types of membranes indicate that at high feed flow rate salt rejection performance diminishes. Nonetheless, both PVDF/h-BN and PVDF membrane exhibit similar increasing trends in permeation flux variation with flow rate. From Fig. 6(b), the permeation fluxes of 12.70 and 18.10 kg/m2h were achieved at feed flow rate of 200 ml/min for PVDF and PVDF/h-BN membranes, respectively. This ratio between the obtained fluxes for both membrane is approximately constant at all flow rates and is equal to around 1.5.

To explain our observed trends, the dependence of the permeation in both membranes to the applied hydrostatic pressure and its independence from the membrane pore structure could be deduced. However, at high flow rates the observed resistance and stability for the hybrid PVDF/h-BN membrane was greater compared to that of the pristine PVDF.

3.3.3 PVDF/h-BN membrane efficiency

The natural seawater sample (from Caspian Sea) was treated through AGMD experiments with PVDF and PVDF/h-BN membranes. The feed temperature and flow rate in all experiments were fixed at 70°C and 200 ml/min, shown in Fig. 7. For better comparison of flux variation in the membranes, the results of both membranes are shown in the same plot with the same measurement times. Permeation flux of the membranes is reduced with time, mainly because of the low soluble minerals and bio-organics on the surface of the membrane. However, in the case of PVDF membrane, the prompt membrane's flux decline is observed. For 15 hours of AGMD operation time, flux of the pristine membrane reaches to about 71% of its initial value. Where in the case of hybrid PVDF/h-BN membrane the permeation flux reduction rates are relatively low (85% of initial value in 15 hours of processing time). This observation indicates that the PVDF/h-BN membrane is more resistant to fouling effects than the pristine PVDF. Nonetheless, the fouling of the membrane pores and subsequent declines in the permeation fluxes are still dominant for the synthesized PVDF/h-BN membrane.

Also, as it is shown in Fig. 7, PVDF/h-BN membranes have a good separation performance during the long-term desalination operation. In fact, regarding to high porosity of PVDF/h-BN membrane, we expect weak mechanical strength and low practical durability. However, the conductivity measurements of the permeate demonstrates salt leaks through the membrane pores after approximately after 13 hours of AGMD process time (from Fig.7). As shown, the increasing in permeate conductivity of PVDF membrane can be attributed to collapse of the pores

structure and pores wetting. On the other hand, the observed stability in the conductivity of PVDF/h-BN permeate stream can be attributed to better durability of PVDF/H-BN membranes.
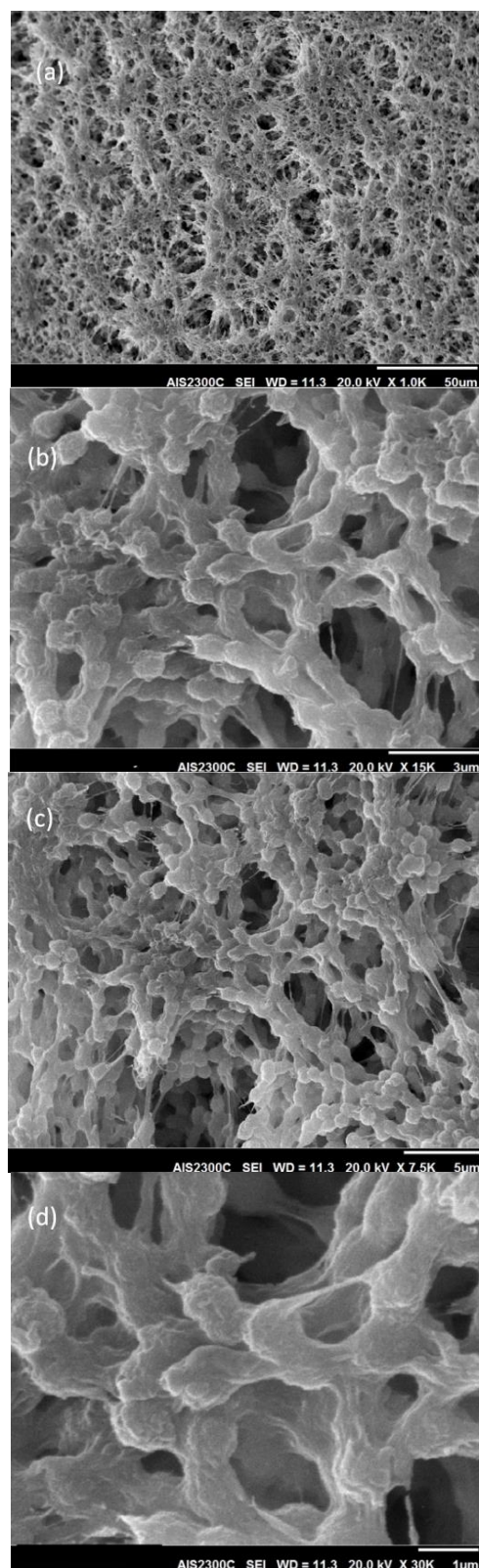

Fig. 5 SEM micrographs of PVDF/h-BN membrane surface prepared through casting in methanol bath at 25˚C
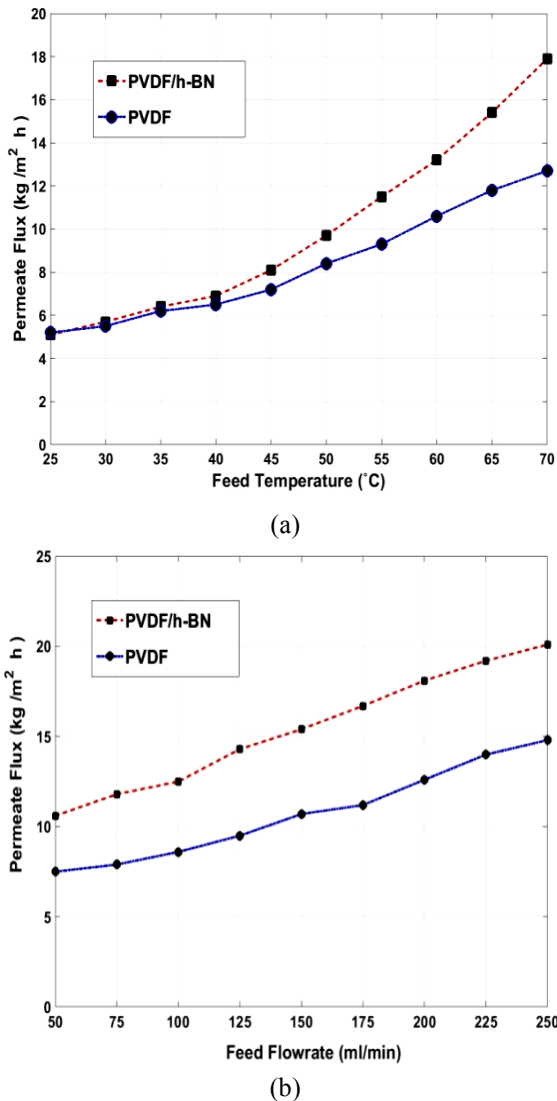
(a)

(b)

Fig. 6 Variation of the synthesized membranes permeation fluxes as a function of (a) feed temperature and (b) feed flow rate
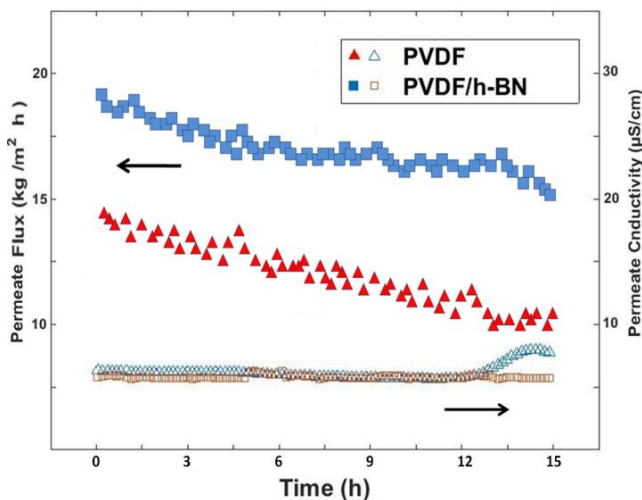

Fig. 7 The durability test results of the PVDF and PVDF/h-BN membranes (square markers are stand for PVDF/h-BN and triangle markers represent the results for PVDF membrane)

The comparison of long-term performances in between the two membranes show that PVDF/h-BN membranes slightly decrease in permeates flux in comparison with pristine PVDF. Moreover, interposing of h-BN platelets into the PVDF membrane induces good separation performance and appropriate durability in AGMD experiments. However, some drawbacks remain pertinent to fouling effects and permeability of this new kind of hybrid membrane which need to be resolved. Considering the simple route presented for synthesis of h-BN platelets as well as distinguished properties of the PVDF/h-BN membrane, this newly introduced hybrid membrane has good potential for desalination purposes. In fact, the prepared membrane diminishes various difficulties relevant to pristine PVDF membrane and exhibit better AGMD performance.

Figs 8(a) and 8(b) indicate the cross-section SEM images of the modified and pristine PVDF membrane. As shown the pristine membrane possesses a dense skin layer with low porosity. However, in the PVDF/h-BN membrane the skin layer is not formed on the top surface of the membrane. The high porosity with uniform pores could be seen in cross section image of PVDF/h-BN hybrid membrane. The elimination of skin layer result in higher surface porosity of hybrid membrane which cause to observation of higher values of permeate flux in MD experiments. As shown in Fig. 8(b) the surface porosity of the new membrane is greater and the pore sizes are likely to be decreased from down to top of membrane. In top surface of the PVDF/h-BN membrane the pores are smaller in comparison to bulk and bottom layer of membrane. In addition, the pore size distribution is low and uniform sizes and shapes of the pores are formed in the PVDF/h-BN membrane. These features of the new membrane directly enhance the membrane separation performance and permeation flux. While in the PVDF membrane the dense skin layer results in high fouling effects and low surface porosity.

For better evaluating of the synthesized membrane operational performance, long-term (10 days) AGMD experiments were conducted by applying seawater as feed at 55°C and 200 ml/min. The permeation flux for both membranes was monitored during the experiments. As illustrated in Fig. 8(c) for both types of membranes the general trend is descending in flux over time. This observation is mainly due to fooling of membrane surface pores. However, in the case of PVDF/h-BN the for around 5 days the sensible reduction in permeation flux was not observed. But for PVDF membrane the fouling effects ate dominant which results in prompt decreasing in permeation flux. In other words, interposing of h-BN nanopowders in polymer matrix diminish the fouling effects by modifying surface porosity and pore sizes. In addition, it results in improving PVDF membrane physical durability in MD operational conditions and enhancing the mechanical strength as well. Fig. 8(d) exhibits the dynamic mechanical analysis (DMA) test plots for both PVDF and PVDF/h-BN membranes. The test results show that the h-BN tended to improve the tensile strength at higher loading. Moreover, the Young's modulus increased in hybrid membrane but in contrast the elongation at max load decreased. These observations demonstrate that the addition of h-BN
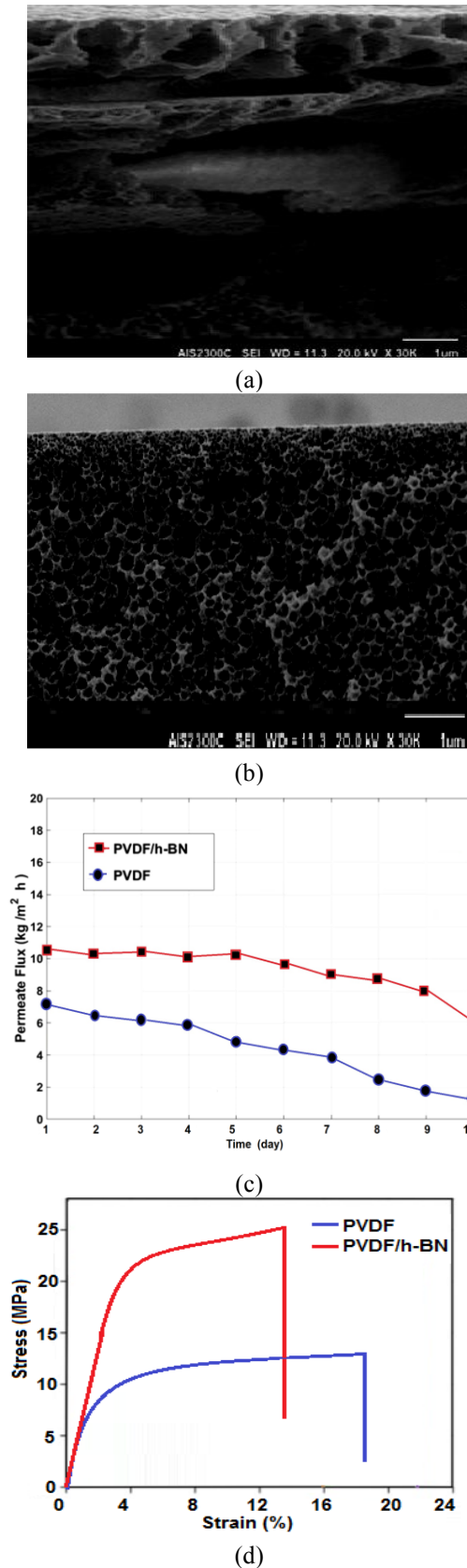
(a)

(b)

(c)

(d)

Fig. 8 Cross section SEM images of (a) PVDF membrane and (b) PVDF/h-BN hybrid membrane. (c) Long-term AGMD test results for permeate flux of PVDF and PVDF/h-BN membranes at 55°C of feed temperature. (d) Dynamic mechanical analysis (DMA) test results for PVDF and PVDF/h-BN membranes

nanoparticles provides extra stiffness to the polymer matrix and increase its mechanical strength.

3.4. Membrane Regeneration

The used PVDF/h-BN membrane was regenerated using ethanol treatment and subsequent drying. For 15 minutes, ethanol (96 v/v%) was filtrated through the membrane in total recycle mode by applying 0.2 bar pressure. Then the membrane was kept in ethanol for 24 hours. Finally, the membrane was dried in oven at 40°C for 48 hours. The regenerated membrane was tested in AGMD mode of operation applying similar feed and conditions explained in section 3.3.

The flux values and conductivity of permeate were measured. As described earlier for 15 hours of operation the permeate flux of PVDF/h-BN membrane was reduced to 85% of its initial value (Fig. 7). After regeneration of the membrane the permeate flux increased to its initial value. Moreover, the conductivity of the permeate was determined to be around 5 μScm^{-1}. These observations indicate that regeneration of PVDF/h-BN membrane was successful.

The effect of compositing membrane with inorganic nanoparticles on permeation flux of MD has been well acknowledged in several studies (Razmju *et al*. 2012, Khayat *et al*. 2015, Moradi *et al*. 2015, Moradi *et al*. 2016 Woo *et al*. 2016). Table 3 illustrate some features of MD membranes which are employed in previous works. In comparison with synthesized membranes mentioned in the literature, the newly developed PVDF/h-BN hybrid membranes in some features such as pore size, porosity and permeability exhibit superior performance. As shown in Table 3, the characteristic features of PVDF/Graphene membrane are comparable with PVDF/h-BN. Considering the cost of graphene and difficulties regarding to graphene nanosheets production, the newly synthesized h-BN nanopowder presents great potential as an appropriate filler in the preparation of hybrid membranes for MD applications.

4. Conclusions

The new type of hybrid membrane was introduced based on compositing of poly(vinylidene fluoride) (PVDF) with hexagonal boron nitride (h-BN) nanosheets. The simple route was presented for production of h-BN powder based on chemical vapor deposition (CVD) process using new boron precursors in nitrogen and hydrogen atmosphere. The synthesized h-BN nanopowder was employed to prepare PVDF/h-BN membrane through phase inversion method. Subsequent characterizations demonstrate the PVDF/h-BN membrane possesses high porosity, hydrophobicity and pore sizes compared to pristine PVDF membrane. Evaluation of the membrane distillation (MD) performance for PVDF/h-BN hybrid membranes and PVDF membranes is experimentally performed. The achieved results indicate that the PVDF/h-BN membrane has competitive salt rejection efficiency in AGMD experiments. Indeed, introduced hybrid membranes exhibit higher MD

Table 3 Properties of some synthesized MD membranes mentioned in literature

Membrane type	MD type	Feed solution	Feed Flow rate (l/min)	Feed Temperature (°C)	Permeate (kg/m²h)	Porosity (%)	Pore size (μm)	Ref.
PVDF/h-BN	AGMD	Real Seawater	0.2	70	18	81	0.22	Present work
PVDF/TiO₂	DCMD	Pure water	1.5	70	17	75	0.40	Razmju *et al.* (2012)
PVDF/SiO₂	VMD	Seawater	Not mentioned	27	3	85	0.14	Efome *et al.* (2015)
PVDF/Graphene	AGMD	Brine water	0.5	60	20	84	0.11	Woo *et al.* (2016)
PVDF	AGMD	Artificial seawater	5.5	70	7	65	0.45	Banat *et al.* (1998)
PVDF	DCMD	Pure water	0.1	70	16	70	0.22	Phattaranawik *et al.* (2003)
PTFE	AGMD	NaCl (3%)	3.3	45	6	70	0.20	Hsu *et al.* (2002)

permeation flux of above 18 kg/m2 h. In addition, the durability results indicate that PVDF/h-BN membrane is more durable and exhibits better stability compared to PVDF, when the real sea water is applied as the feed.

References

Al-Obaidani, S., Curcio, E., Macedoniob, F., Di Profiob, G., Al. Hinaid, H. and Drioli, E. (2008), "Potential of membrane distillation in seawater desalination: Thermal efficiency, sensitivity study and cost estimation", *J. Membr. Sci.*, **323**(1), 85-98.

Al-Shammiri, M., Safar, M. and Al-Dawas, M. (2000), "Evaluation of two different antiscalants in real operation at the Doha research plant", *Desalination*, **128**(1), 1-16.

Banat, F.A. and Simandl, J., (1998), "Desalination by membrane distillation: A parametric study", *Sep. Sci. Technol.* **33**(2), 201-226.

Bottino, A., Capannelli, G., Comite, A., Costa, C., Calvo, J.I. and Saelee. R. (2015), "Novel polytetrafluoroethylene tubular membranes for membrane distillation", *Desalination Water Treat.*, **53**(6), 1559-1564.

Chang, H., Hung, C.Y., Chang, C.L., Cheng, T.W. and Ho, C. D. (2015), "Optimization of three small-scale solar membrane distillation desalination systems", *Membr. Water Treat.*, **6**(6), 451-476.

Chang, H.H., Tsai, C.H., Wei, H.C. and Cheng, L.P. (2014), "Effect of structure of PVDF membranes on the performance of membrane distillation", *Membr. Water Treat.*, **5**(1), 41-56.

Choi, S.R., Bansal, N.P. and Garg, A. (2007), "Mechanical and microstructural characterization of boron nitride nanotubes-reinforced SOFC seal glass composite", *Mater. Sci. Eng. A*, **460**, 509-515.

Chung, T.S. (1996), "A review of microporous composite polymeric membrane technology for air separation", *Polym. Polym. Compos.*, **4**(4), 269-283.

Ciofani, G., Raffa, V., Menciassi, A. and Cuschieri, A. (2008), "Cytocompatibility, interactions and uptake of polyethyleneimine-coated boron nitride nanotubes by living cells: Confirmation of their potential for biomedical applications", *Biotechnol. Bioeng.*, **101**(4), 850-858.

Criscuoli, A., Bafaro, P. and Drioli, E. (2013), "Vacuum membrane distillation for purifying waters containing arsenic", *Desalination*, **323**(8), 17-21.

Criscuoli, A. and Drioli, E. (1999), "Energetic analysis of an integrated membrane desalination", *Desalination*, **124**(1-3), 243-249.

Darwish, M.A., Al-Najem and N.M. (2000), "Energy consumption by multi-stage flash and reverse osmosis desalters", *App. Therm. Eng.*, **20**(5), 399-416.

Dastbaz, A., Karimi-Sabet, J., Ahadi, H. and Amini, Y. (2017), "Preparation and characterization of novel modified PVDF-HFP/GO/ODS composite hollow fiber membrane for Caspian Sea water desalination", *Desalination*, **424**(12), 62-73.

Duan, J., Xue, R., Xu, Y. and Sun, Ch. (2008), "Preparation of boron nitride flakes by a simple powder reaction", *J. Amer. Ceramic Soc.*, **91**(7), 2419-2418.

Efome, J.E., Baghbanzadeh, M., Rana, D., Matsuura, T. and Lan, C.Q. (2015), "Effects of superhydrophobic SiO₂ nanoparticles on the performance of PVDF at sheet membranes for vacuum membrane distillation", *Desalination*, **373**(10), 47-57.

Guillén-Burrieza, E., Blanco, J. and Zaragoza, G. (2011), "Experimental analysis of an air gap membrane distillation solar desalination pilot system", *J. Membr. Sci.*, **379**(1-2), 386-396.

Hao, X., Yub, M., Cui, Z., Xu, X., Wang, Q. and Jiang, M. (2002), "The Effect of temperature on the synthesis of BN nanoscrystals", *J. Crys. Growth*, **241**(1-2), 124-128.

Hossain, M.M. (2013), "Treatment of ground waters in a hollow-fibre liquid membrane contactor for removal of ions", *Membr. Water Treat.*, **4**(2), 95-108.

Hsu, S.T., Cheng, K.T. and Chiou, J.S. (2002), "Seawater desalination by direct contact membrane distillation", *Desalination*, **143**(3), 279-287.

Huayan, C., Chunrui, W., Yue, J., Xuan, W. and Xiaolong, L. (2011), "Comparison of three membrane distillation configurations and seawater desalination by vacuum membrane distillation", *Desalination Water Treat.*, **28**(1-3), 321-327.

Hubacek, M. and Ueki, M. (1996), "Chemical reactions in hexagonal boron nitride system", *J. Solid State Chem.*, **123**(2), 215-222.

Hubacek, M., Sato, T. and Ishii, T. (1994), "A coexistence of boron nitride and boric oxide", *J. Solid State Chem.*, **109**(2), 384-390.

Khayet, M., Mengual, J. and Matsuura, T. (2005), "Porous hydrophobic/hydrophilic composite membranes: application in desalination using direct contact membrane distillation", *J. Membr. Sci.*, **252**(1-2), 101-113.

Kim, D.H., Fasulo, P.D., Rodgers, W.R. and Paul, D.R. (2008), "Effect of the ratio of maleated polypropylene to organoclay on the structure and properties of TPO-based nanocomposites. Part II: thermal expansion behavior," *Polymer*, **49**(10), 2492-2506.

Koo, J., Han, J., Sohn, J., Lee, S. and Hwang T.M. (2013), "Experimental comparison of direct contact membrane distillation (DCMD) with vacuum membrane distillation (VMD)", *Desalination Water Treat.*, **51**(31-33), 6299-6309.

Lau, W.J., Goh, P.S. Ismail, A.F. and Lai S.O. (2011), "Ultrafiltration as a pretreatment for seawater desalination: A review", *Membr. Water Treat.*, **5**(1), 5-29.

Lee, H.S., Fasulo, P.D., Rodgers, W.R. and Paul, D.R. (2006), "TPO based nanocomposites. Part 2. Thermal expansion behavior", *Polymer*, **47**(10), 3528-3539.

Loussif, N. and Orfi, J., (2016) "Comparative study of air gap,

direct contact and sweeping gas membrane distillation configurations", *Membr. Water Treat.*, **7**(1), 71-86.

Molinari, R. and Argurio, P. (2011), "Recent progress in supported liquid membrane technology: stabilization and feasible applications", *Membr. Water Treat.*, **2**(4), 207-223.

Moradi, R., Karimi, J., Shariaty-Niassar, M. and Amini, Y. (2016), "Experimental investigation of nanofibrous poly(vinylidene fluoride) membranes for desalination through air gap membrane distillation process", *Korean J. Chem. Eng.*, **33**(10), 2953-2960.

Moradi, R., Karimi-Sabet, J., Shariaty-Niassar, M. and Hedayat, S.M. (2017), "Synthesis and preparation of mono-layer h-BN nanopowders by using a combination of CVD method with isopropanol-assisted exfoliation process", *Powder Metall. Met. C+*, **55**(9-10), 530-541.

Moradi, R., Karimi-Sabet, J., Shariaty-Niassar, M. and Koochaki, M.A. (2015), "Preparation and characterization of polyvinylidene fluoride/graphene superhydrophobic fibrous films", *Polymers*, **7**(8), 1444-1463.

Moradi, R., Monfared. S.M., Amini, Y. and Dastbaz, A. (2016), "Vacuum enhanced membrane distillation for trace contaminant removal of heavy metals from water by electrospun $PVDF/TiO_2$ hybrid membranes", *Korean J. Chem. Eng.*, **33**(7), 2160-2168.

Phattaranawik, J., Jiraratananon, R. and Fane, A.G. (2003), "Heat transport and membrane distillation coefficients in direct contact membrane distillation", *J. Membr. Sci.*, **212**(1-2), 177-193.

Qtaishat, M., Rana, D., Khayet, M. and Matsuura, T., (2009), "Preparation and characterization of novel hydrophobic/hydrophilic polyetherimide composite membranes for desalination by direct contact membrane distillation", *J. Membr. Sci.*, **327**(1-2), 264-273.

Razmjou, A., Arifin, E., Dong, G., Mansouri J. and Chen V. (2012), "Superhydrophobic modification of TiO_2 nanocomposite PVDF membranes for applications in membrane distillation", *J. Membr. Sci.*, **415**(10), 850-863.

Shi, L., Gu, Y.L., Chen, L.Y., Yang, Z.H., Ma, J.H. and Qian, Y.T. (2004), "Formation of nanocrystalline BN with a simple chemical route", *Mater. Lett.*, **58**(26), 3301-3308.

Shoaie, R., Karimi-Sabet, J., Mousavian, S.M.A., Khadiv-Parsi, P. and Moradi, R. (2017), "Optimal modification of poly(vinylidene fluoride) membrane surface by using surface-modifying macromolecules for application in membrane distillation", *J. Des. Water Treat.*, **71**(5), 62-78

Smolders, K. and Franken, A.C.M. (1989), "Terminology for membrane distillation", *Desalination*, **72**(3), 249-262.

Van der Bruggen, B. (2003), "Desalination by distillation and by reverse osmosis, trends towards the future", *Membr. Tech.*, **2003**(2), 6-9.

Woo, Y.C., Kim, Y., Shim, W.G., Tijing L.D., Yao, M., Nghiem L.D., Choi, J.S., Kim, S.H. and Shon H.K. (2016), "Graphene/PVDF flat-sheet membrane for the treatment of RO brine from coal seam gas produced water by air gap membrane distillation", *J. Membr. Sci.*, **513**(9), 74-84.

Wu, X., Zhao, B., Wang, L., Zhang, Z., Zhang, H., Zhao, X. and Guo, X. (2016), "Hydrophobic PVDF/graphene hybrid membrane for CO_2 absorption in membrane contactor", *J. Membr. Sci.*, **520**(12), 120-129.

Yu, Y., Chen, H., Liu, Y., Craig, V.S.J., Wang, Ch., Li, L.H. and Chen, Y. (2015), "Superhydrophobic and superoleophilic porous boron nitride nanosheet/polyvinylidene fluoride composite material for oil-polluted water cleanup", *Adv. Mater. Interfaces*, **2**(1), 1400267-1400277.

Zha, D., Mei, S., Wang, X., Li, H., Shi, Z. and Jin, Z. (2011), "Superhydrophobic polyvinylidene fluoride/graphene porous materials", *Carbon*, **49**(15), 5166-5172.

Zhi, C., Bando, Y., Tang, C., Honda, S., Kuwahara, H. and Golberg, D. (2006), "Boron nitride nanotubes/polystyrene composites", *J. Mater. Res.*, **21**(11), 2794-2800.

Zhi, C., Bando, Y., Tang, C., Honda, S., Sato, K. and Kuwahara, H. (2005), "Characteristics of boron nitride nanotube-polyaniline composites", *Angew. Chem.*, **44**(48), 7929-7932.

Zoungrana, A., Zengin, I.H., Elcik, H., Yeshilırmak, D., Karadagh, D. and Chakmakci, M. (2016), "Arsenic removal from drinking water by direct contact membrane distillation", *Membr. Water Treat.*, **7**(3), 241-255.

CC